ADVANCED FUNCTIONAL MATERIALS
www.afm-journal.de

Air-Stable n-Type Organic Field-Effect Transistors Based on Carbonyl-Bridged Bithiazole Derivatives

By *Yutaka Ie,* Masashi Nitani, Makoto Karakawa, Hirokazu Tada,* and *Yoshio Aso**

An electronegative conjugated compound composed of a newly designed carbonyl-bridged bithiazole unit and trifluoroacetyl terminal groups is synthesized as a candidate for air-stable n-type organic field-effect transistor (OFET) materials. Cyclic voltammetry measurements reveal that carbonyl-bridging contributes both to lowering the lowest unoccupied molecular orbital energy level and to stabilizing the anionic species. X-ray crystallographic analysis of the compound shows a planar molecular geometry and a dense molecular packing, which is advantageous to electron transport. Through these appropriate electrochemical properties and structures for n-type semiconductor materials, OFET devices based on this compound show electron mobilities as high as 0.06 $cm^2 V^{-1} s^{-1}$ with on/off ratios of 10^6 and threshold voltages of 20 V under vacuum conditions. Furthermore, these devices show the same order of electron mobility under ambient conditions.

1. Introduction

Considerable efforts have been devoted to developing new π-conjugated systems as active materials for organic field-effect transistors (OFETs) because of their potential application in low-cost, large-area, and flexible electronic devices.[1] Significant progress has recently been made in the development of p-type OFET materials.[2] However, limited studies have been conducted on the development of n-type OFET materials.[3–14] This is because of the insufficiency of their molecular design in stabilizing electron-injected species and arranging the molecular ordering for efficient electron transport in the solid state. Moreover, although an improvement in device stability under ambient conditions is highly desirable for practical applications in OFETs, only a few π-conjugated systems, such as halogenated phthalocyanine,[15] acene carboxylic diimide,[16–22] dicyanomethylene-substituted conjugated compounds,[23,24] and perfluoroalkyl-substituted fullerenes,[25] are known to operate as air-stable n-type OFET materials.

[*] Dr. Y. Ie, Prof. Y. Aso, M. Nitani, Dr. M. Karakawa
The Institute of Scientific and Industrial Research
Osaka University
8-1, Mihogaoka, Ibaraki, Osaka 567-0047 (Japan)
E-mail: yutakaie@sanken.osaka-u.ac.jp; aso@sanken.osaka-u.ac.jp
Prof. H. Tada
The Graduate School of Engineering Science
Osaka University
1-3, Machikaneyama, Toyonaka, Osaka 560-8531 (Japan)

DOI: 10.1002/adfm.200901803

Recently, we have reported that the presence of trifluoroacetyl groups at the terminal positions of a π-conjugated oligomer is effective in both lowering the lowest unoccupied molecular orbital (LUMO) energy level and invoking strong intermolecular interactions.[26] We have also reported that this terminal group combined with 5,5′-diphenyl-2,2′-bithiophene exhibits good n-channel characteristics when used in an OFET device.[27] On the basis of these findings, we anticipated that if an electron-accepting π-conjugated unit is utilized instead of the electron-donating bithiophene, then the n-type character would be further enhanced, thus contributing to the stabilization of device operation under ambient conditions. On the other hand, Yamashita et al. have demonstrated that π-conjugated oligomers containing electron-accepting thiazole rings exhibit a high performance as n-type OFET materials.[6] However, the OFET characteristics of these oligomers were not observed under ambient conditions. With these studies in mind, we have focused on the introduction of carbonyl bridging, because carbonyl bridging of biaryls is known to cause a decrease in the LUMO energy level.[9ad,11,13] Therefore, in this study, we have designed a carbonyl-bridged bithiazole as a new electronegative unit intended for combining with trifluoroacetyl terminal groups. We first calculated the molecular orbitals of carbonyl-bridged conjugated compound **C-BTz** and nonbridged **BTz** by density functional theory (DFT) at the B3LYP/6-31G(d,p) level. As depicted in Figure 1, the carbonyl group more strongly participates in the LUMO of **C-BTz** than its highest occupied molecular orbital (HOMO), and as a consequence **C-BTz** possesses a notably lower LUMO energy level

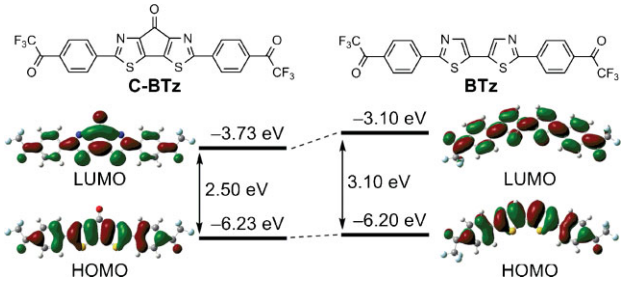

Figure 1. Chemical structures and HOMO and LUMO energies calculated using DFT at the B3LYP/6-31G(d,p) level.

than nonbridged **BTz**. In this article, we report on the synthesis, properties, and n-type OFET performance of **C-BTz**. Furthermore, the effect of carbonyl bridging is ascertained by comparing the properties of **C-BTz** with those of nonbridged **BTz**.

2. Results and Discussion

2.1. Synthesis, Properties, and Structures

As shown in Scheme 1, carbonyl-bridged bis(triisopropylsilyl)-bithiazole **2** was synthesized by lithiation of **1** with lithium diisopropylamide (LDA) and subsequent treatment with ethyl 1-piperidine carboxylate, after which it was converted into a stannylated bithiazole derivative **4** via acetal protection[28] of the carbonyl group. The newly designed target compound **C-BTz** was prepared by a Stille-coupling reaction of **4** with 4′-bromo-2,2,2-trifluoroacetophenone and subsequent acidic acetal deprotection. A similar cross-coupling procedure was applied to the synthesis of reference compound **BTz**. Both the final compounds were purified by gradient sublimation under a high vacuum and unambiguously characterized by mass spectrometry (MS), nuclear magnetic resonance (NMR) spectroscopy, and elemental analysis (see Experimental section and Supporting Information (SI)).

The electrochemical properties of the obtained conjugated compounds were investigated by cyclic voltammetry (CV) measurements, which were carried out at a scan rate of 100 mV s^{-1} in fluorobenzene containing 0.1 M tetrabutylammonium hexafluorophosphate ($TBAPF_6$) as the supporting electrolyte. A platinum disk was used as the working electrode, a platinum wire as the counter electrode, and $Ag/AgNO_3$ as the reference electrode. As shown in Figure 2a, carbonyl bridging caused a large positive shift of 0.47 V in the first reduction potential. Furthermore, in contrast to the irreversible reduction wave for **BTz**, **C-BTz** showed two reversible reduction waves with half-wave potentials $E_{1/2}^{red} = -1.16$ and -1.53 V. These phenomena clearly indicate that carbonyl bridging contributes considerably to not only an increase in electron affinity but also to kinetically stabilizing of the anionic species. From the first reduction potential of **C-BTz** and under the premise that the energy level of ferrocene/ferrocenium (Fc/Fc^+) is -4.8 eV below the vacuum level, the LUMO energy level of **C-BTz** is estimated to be -3.64 eV,[29] which is fairly consistent with the calculated value (-3.73 eV) (Fig. 1).

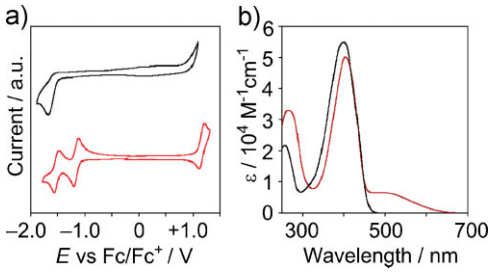

Figure 2. a) Cyclic voltammograms of **C-BTz** (red) and **BTz** (black) in fluorobenzene containing 0.1 M $TBAPF_6$. b) UV–vis absorption spectra of **C-BTz** (red) and **BTz** (black) in THF.

As shown in Figure 2b, the UV–vis absorption spectrum of **BTz** in tetrahydrofuran (THF) exhibited an absorption maximum related to the HOMO–LUMO transition at 405 nm. Interestingly, introduction of carbonyl bridging leads to the appearance of a shoulder at around 550 nm.[26] According to time-dependent DFT calculations at the B3LYP/6-31G(d,p) level, this shoulder can be mainly ascribed to the HOMO–LUMO transition with an oscillator strength (f) of 0.29. This result indicates that the optical HOMO–LUMO energy gap of **C-BTz** is smaller than that of **BTz**, which can be explained by the lowering of the LUMO energy level (Fig. 1). The intense absorption band of **C-BTz** at 405 nm is similarly related to the HOMO–LUMO+1 transition ($f = 1.18$).

To better understand the molecular structure and packing diagram in the solid state, X-ray crystallographic analysis of **C-BTz** was carried out. Single crystals were grown from a $CHCl_3$ solution by slow evaporation. The X-ray crystallographic analysis confirmed that the **C-BTz** molecule exhibits a planar geometry, with dihedral angles between the thiazole rings and between the thiazole and phenyl rings of around 0.5° and 12°, respectively (Fig. 3a). As expected, both the carbonyl groups in the molecule have a significant influence on the molecular arrangement. As shown by the dashed lines in Fig. 3b, the carbonyl-bridged bithiazole and terminal trifluoroacetyl groups induce several short contacts between adjacent molecules, resulting in a dense π-stacked packing along the *b*-axis with interplanar distances of 3.40 and 3.52 Å. On the basis of this packing structure, the intermolecular transfer integrals (t) of the HOMOs and LUMOs between

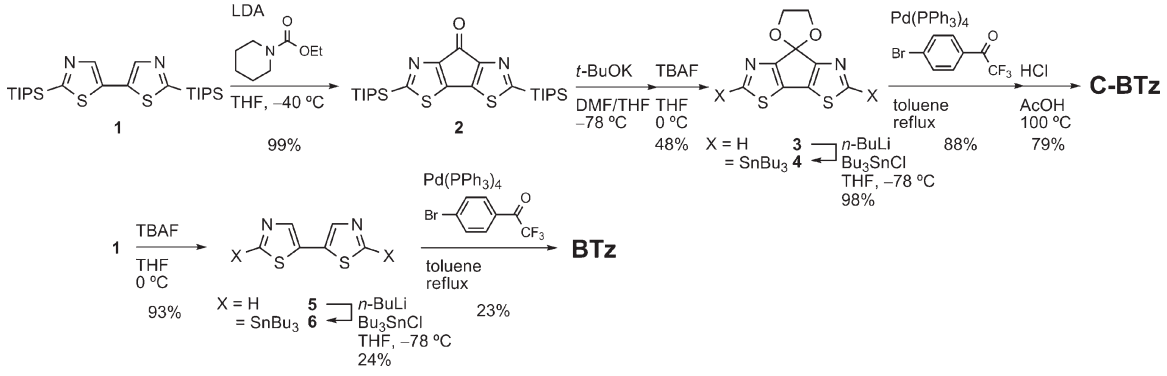

Scheme 1. Synthesis of **C-BTz** and **BTz**.

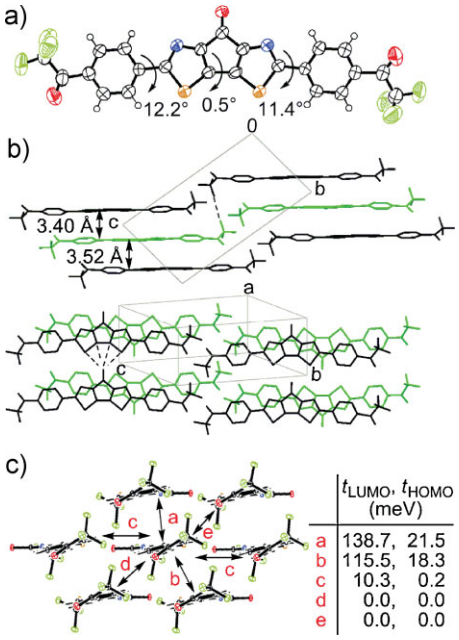

Figure 3. a) Molecular structure and b) packing diagram of **C-BTz**. Dashed lines indicate contacts shorter than the sum of van der Waals radii. c) Estimated transfer integrals of HOMO and LUMO energy levels between neighboring molecules viewed along the long molecular axis.

neighboring molecules were estimated by an extended Hückel molecular orbital calculation.[30] The calculations were independently carried out for the HOMOs and LUMOs of the molecules. As shown in Fig. 3c, the calculated transfer integrals of the LUMOs are one magnitude larger than those of the HOMOs, and large overlaps were observed along the π-stacked direction. This result implies that efficient electron transport along the *b*-axis is favorable for the **C-BTz** crystals.

2.2. Field-Effect Properties and Morphologies of the Thin Films

The semiconductor performances of these conjugated compounds were evaluated in OFETs with bottom-contact and top-contact geometries. OFET devices were fabricated on the gate electrode of a p-doped silicon substrate. Source and drain gold electrodes with a channel width/channel length (W/L) of 38 mm/5 μm were prepatterned on a 300 nm layer of SiO_2 dielectrics for OFETs with bottom-contact geometry. Films of **C-BTz** or **BTz** were vacuum-deposited after octadecyltrichlorosilane (ODTS) treatment of the substrate. OFET devices with top-contact geometry were fabricated by patterning the gold electrodes over organic thin films using a shadow mask to achieve a W/L of 5 mm/20 μm. The deposition of the organic films was carried out at different substrate temperatures and various annealing temperatures were investigated and optimized for all the devices. FET parameters obtained from measurements under vacuum conditions are summarized in Table 1. All the devices showed typical n-channel characteristics, and among them, the **C-BTz**-based device displayed a superior FET performance with a maximum electron mobility of 0.06 cm^2 V^{-1} s^{-1}, which is almost two orders of magnitude higher than that of **BTz** (runs 1 and 7). Its output and transfer characteristics are shown in Figure 4.[31] It is important to note that the **C-BTz**-based device showed the same order of electron mobility irrespective of the device geometry, indicating the potential versatility for practical device fabrication (runs 1, 2). To examine the stability of the **C-BTz**-based OFET under the biased conditions, the top-contact device was repeatedly biased by sweeping the gate voltage (V_{GS}) from −20 to 50 V under a fixed source–drain voltage (V_{DS}) of 50 V, and its source–drain current (I_{DS}) was monitored. As shown in Figure 5, the transfer curves showed little hysteresis under dual sweep conditions and an almost unchanged electrical performance even after 500 cycles, demonstrating a high stability under operating conditions. Thus, **C-BTz** is a promising semiconductor for practical OFET applications.

The morphology and structural order of the **C-BTz** and **BTz** thin films on SiO_2 substrates fabricated under the conditions of runs 1 and 7 in Table 1, respectively, were investigated by atomic force microscopy (AFM) and X-ray diffraction (XRD). The AFM image of the **C-BTz** film showed uniform grains that are tightly connected to each other (Fig. 6a), while the **BTz** film revealed comparatively large crystalline grains of several micrometers in size and clearly observable grain boundaries (Fig. 6b). In contrast to their different morphologies, the XRD measurements of both the films exhibited sharp reflections (Fig. 6c,d), indicating the crystallinity of both thin films. However, the peak intensities of the **BTz** film were weaker than those of the **C-BTz** film and, together with a series of peaks at a *d*-spacing of around 14.4 Å, weak peaks corresponding to different

Table 1. Field-effect characteristics of **C-BTz** and **BTz** in vacuum and in air.

Run	Compound	T_D [°C] [a]	T_A [°C] [b]	Measurement conditions	μ [$cm^2V^{-1}s^{-1}$]	I_{on}/I_{off}	V_{th} [V]
1	**C-BTz**[c]	110	210	Under vacuum	0.06	10^6	20
2	**C-BTz**[d]	110	130	Under vacuum	0.03	10^3	33
3	**C-BTz**[d]	110	130	In air	0.014	10^4	44
4	**C-BTz**[d]	110	130	In air	0.013[e]	10^6	68
5	**C-BTz**[d]	110	130	In air	6.1×10^{-5}[f]	10	61
6	**C-BTz**[d]	110	130	Under vacuum	4.6×10^{-3}[f]	10^5	73
7	**BTz**[c]	90	150	Under vacuum	7.1×10^{-4}	10^4	15
8	**BTz**[d]	90	110	Under vacuum	2.0×10^{-3}	10^4	57
9	**BTz**[d]	90	110	In air	No FET		

[a] Substrate deposition temperature. [b] Annealing temperature. [c] Bottom-contact geometry. [d] Top-contact geometry. [e] After 24 h. [f] After 1 year.

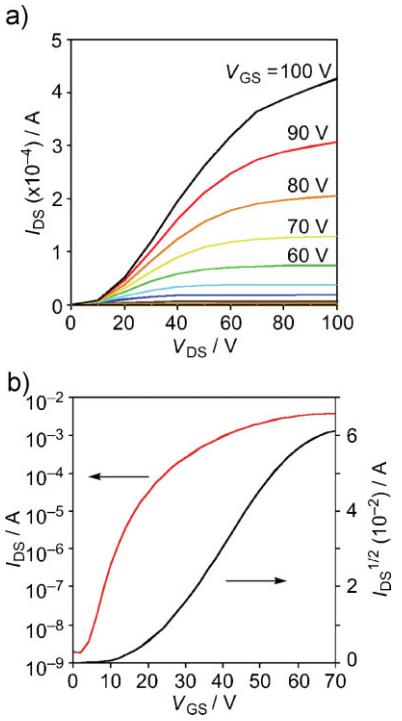

Figure 4. a) Output characteristics of a bottom-contact OFET using **C-BTz**. b) Transfer characteristics of the same device at drain voltage of 100 V. I_{DS}, V_{DS}, and V_{GS} denote source–drain current, source–drain voltage, and gate voltage, respectively.

d-spacings were also observed (inset in Fig. 6d), indicating that **BTz** crystals and/or molecules are randomly orientated between the grains.[32] In addition to the relatively high LUMO energy level compared to that of **C-BTz**, this observation as well as the large grain boundaries might be accountable for the moderate electron mobility of the **BTz**-based devices. On the other hand, the film of **C-BTz** showed well distinguishable reflection peaks up to the third order corresponding to a *d*-spacing of 18.0 Å, which is almost equal to the length (17.7 Å) of the crystallographic *c*-axis. XRD simulations calculated from crystallographic data of **C-BTz** were very similar (Fig. S3 (SI)) to the observed XRD patterns. These results suggest that the molecules possess a stacking orientation parallel to the SiO_2 surface, which certainly contributes to the high field-effect electron mobility of the **C-BTz** films.

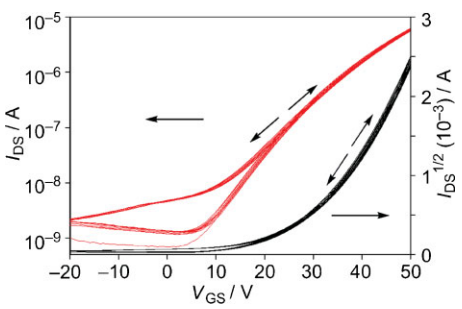

Figure 5. Transfer characteristics of a top-contact OFET using **C-BTz** with repeated biases for up to 500 cycles at a source–drain voltage of 50 V.

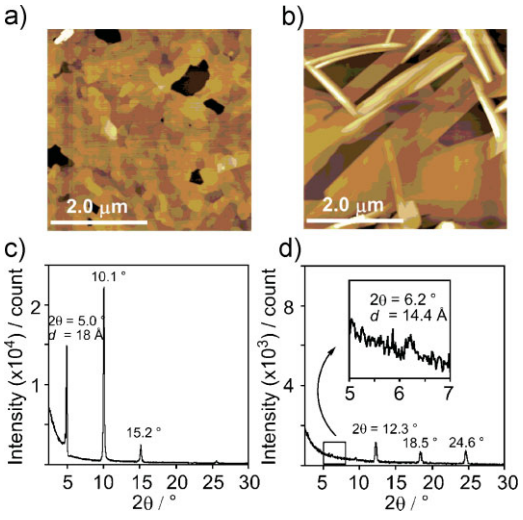

Figure 6. a,b) AFM images of a **C-BTz** film (a) and a **BTz** film (b) on SiO_2. c,d) XRD data of c) a **C-BTz** film and d) a **BTz** film on SiO_2.

Finally, the device stability of the **C-BTz**- and **BTz**-based OFETs with top-contact geometry was investigated under ambient atmospheric conditions. As shown in runs 2 and 3 in Table 1 and Figure 7, the **C-BTz**-based device showed n-channel characteristics with an electron mobility of the same order of magnitude as that measured under vacuum conditions, and its performance was maintained even after storage under ambient conditions for 24 h (runs 3 and 4, Table 1). In contrast, the FET response of the **BTz**-based device completely disappeared (run 9, Table 1). There have been several argumentations about the air stability of n-channel OFETs in terms of the LUMO energy levels of the semiconductors and their formal redox potential for H_2O, and it has been suggested that compounds having a lower LUMO level than −4.0 eV should be advantageous for gaining air stability.[24b,33,34] Despite the higher estimated LUMO energy level (−3.64 eV) of **C-BTz**, OFET devices based on **C-BTz** show a fairly high stability under ambient conditions as described above. This air stability of **C-BTz**-based devices is attributable to both the kinetic stability of the anionic species and the high crystallinity with dense favorable arrangements, which apparently originates from the presence of carbonyl bridging as well as the trifluoroacetyl terminal groups. After storage of the device under ambient atmospheric conditions for 1 year the

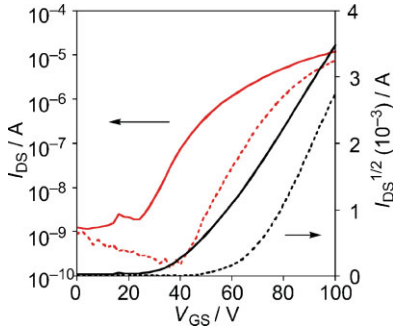

Figure 7. Transfer characteristics of a top-contact OFET using **C-BTz** measured in air (solid line) and after 24 h of storage in air (dashed line).

electron mobility and on/off current ratio measured in air decreased to 6.1×10^{-5} cm^2 V^{-1} s^{-1} and 10, respectively (run 5 in Table 1, and Fig. S4a (SI)). However, the electron mobility could be improved by two orders of magnitude and an initial on/off current ratio of 10^5 could be obtained when carrying out the measurements under a reduced pressure of 10^{-6} Pa (run 6 in Table 1, and Fig. S4b (SI)). However, the threshold voltage (V_{th}) was much higher (positive shift) with increasing storage period in air and could not be recovered even under vacuum conditions.[35] These results indicate that, although reversibly, physically adsorbed oxygen and/or water do degrade the device performance, the **C-BTz** molecule does have an intrinsic air stability when used as an active material for n-channel OFETs. The positive shift of V_{th} accompanied by a change in the electron mobility and on/off current ratio might be ascribable to the formation of deep traps at the semiconductor/insulator interface and/or at the grain boundaries.[3a]

3. Conclusions

We have successfully designed and synthesized carbonyl-bridged bithiazole as a new electronegative unit and developed a carbonyl-bridged-bithiazole-based conjugated molecule **C-BTz**. Results of spectroscopic and electrochemical measurements and X-ray analysis of **C-BTz** revealed that the combination of carbonyl-bridging and electron-accepting thiazole rings contributes to a low LUMO energy level and an appropriate molecular structure and arrangement for charge-carrier transport. Because of this low LUMO energy level and high transfer integrals, the **C-BTz**-based OFET devices exhibited one of the highest levels of n-type performances and air stability. Our study showed that this simple modification of molecules could not only facilitate the improvement in device performance but also increase the device stability under ambient conditions, which will provide possibilities for further development of a new category of n-type semiconductor materials. We are currently investigating further improvements in the performance of **C-BTz**-based OFET devices by optimizing the device structure, metal electrodes, and gate dielectrics, as well as using surface treatments.

4. Experimental

General Information: Column chromatography was performed on silica gel (KANTO Chemical silica gel 60N, 40–50 μm) or neutral alumina (Merck aluminum oxide 90 standardized). Thin-layer chromatography (TLC) plates were visualized with UV. Preparative gel-permeation chromatography (GPC) was performed on a Japan Analytical Industry LC-908 equipped with a JAI-GEL 1H/2H. Melting points are reported uncorrected. ^{1}H NMR and ^{13}C NMR spectra were recorded on a JEOL LA-400 and LA-600 in $CDCl_3$ with tetramethylsilane as an internal standard. Data are reported as follows: chemical shift in ppm (δ), multiplicity (s = singlet, d = doublet, t = triplet, m = multiplet), coupling constant (Hz), and integration. Mass spectra were obtained on a Shimadzu GCMS-QP-5050. UV–vis spectra were recorded on a Shimadzu UV-3100PC. Fluorescence spectra were recorded using a Fluoromax-2 spectrometer in the photocounting mode equipped with a Hamamatsu R928 photomultiplier. The bandpass for the emission spectra was 1.0 nm. Fluorescence quantum efficiencies were measured using diphenylanthracene ($\Phi_f = 0.90$ in cyclohexane) as a standard. The concentrations of solutions were adjusted to yield an absorptivity of $A < 0.1$ in the absorption spectrum for any fluorescence experiments. All spectra were obtained in spectrograde solvents. Cyclic voltammetry was carried out on a BAS CV-620C voltammetric analyzer. Elemental analyses were performed on a PerkinElmer LS-50B by the Elemental Analysis Section of the Comprehensive Analysis Center (CAC) of The Institute of Scientific and Industrial Research (ISIR), Osaka University. The surface structure of the deposited organic film was observed by AFM (Shimadzu, SPM9600), and the film crystallinity was evaluated by XRD (Rigaku, RINT2500). XRD patterns were obtained using a Bragg–Brentano geometry with Cu Kα radiation as an X-ray source with an acceleration voltage of 50 kV and a beam current of 200 mA. The XRD patterns were carried out in the scanning mode using θ–2θ scans between 2.5° and 40° with scanning step of 0.02°.

Materials: All reactions were carried out under a nitrogen atmosphere. Solvents of the highest purity grade were used as received. Unless stated otherwise, all reagents were purchased from commercial sources and used without purification. 5-Bromo-2-(triisopropylsilyl)thiazole was prepared by the reported procedure [36]. The ^{1}H NMR data of 5-bromo-2-(triisopropylsilyl)thiazole was in agreement with that previously reported.

Synthesis of **1**: 5-Bromo-2-(triisopropylsilyl)thiazole (8.60 g, 26.8 mmol), 5-(tri-*n*-butylstannyl)-2-(triisopropylsilyl)thiazole (15.0 g, 28.3 mmol), and tetrakis(triphenylphosphine)palladium(0) (930 mg, 0.839 mmol) were placed in a 200 mL round-bottomed flask and dissolved in toluene (90 mL). The reaction mixture was stirred at 120 °C for 17 h. After being cooled to room temperature, the reaction mixture was filtered over celite. After removal of the solvent under reduced pressure, the residue was purified by column chromatography on alumina (20:1 hexane/EtOAc) to give **1** (11.6 g, 90%) as a white solid: m.p. 138–139 °C; ^{1}H NMR (400 MHz, $CDCl_3$) δ [ppm]: 8.19 (s, 2H), 1.46 (m, 6H), 1.16 (d, 36H, $J = 7.5$ Hz); ^{13}C NMR (150 MHz, $CDCl_3$) δ [ppm]: 170.6, 143.3, 131.0, 18.4, 11.7; MS (EI) *m/z* 480 [M^+]. Anal. calcd. for $C_{24}H_{44}N_2S_2Si_2$: C 59.94, H 9.22, N 5.82; found: C 60.11, H 9.42, N, 5.74.

Synthesis of **2**: Diisopropylamine (0.8 mL, 58 mmol) and THF (1 mL) were placed in a 50 mL round-bottomed flask. To the mixture was added dropwise *n*-BuLi (1.58 M, 3.2 mL, 5.1 mmol) at −78 °C, and the resulting mixture was allowed to warm up to 0 °C for 30 min. After cooling the mixture back down to −40 °C, **1** (385 mg, 0.801 mmol) in THF (20 mL) was added dropwise to it. After stirring for 1 h at −40 °C, ethyl-1-piperidinecarboxylate (200 mg, 1.27 mmol) in THF (8 mL) was added. After further stirring for 1 h at −40 °C, the reaction was quenched by addition of H_2O (5 mL). The aqueous layer was extracted with EtOAc, and the combined organic layers were washed with water and dried over $MgSO_4$. After removal of the solvent under reduced pressure, the residue was purified by column chromatography on silica gel (hexane) to give **2** (401 mg, 99%) as a red solid: m.p. 162–163 °C; ^{1}H NMR (400 MHz, $CDCl_3$) δ [ppm]: 1.45 (m, 6H), 1.15 (d, 36H, $J = 7.5$ Hz); ^{13}C NMR (150 MHz, $CDCl_3$) δ [ppm]: 179.1, 174.0, 158.1, 145.3, 18.5, 11.5; MS (EI) *m/z* 506 [M^+]. Anal. calcd. for $C_{25}H_{42}N_2OS_2Si_2$: C 59.23, H 8.35, N 5.53; found: C 59.27, H 8.64, N 5.25.

Synthesis of **3**: To a solution of **2** (3.00 g, 5.91 mmol) and 2-chloroethanol (1.90 g, 23.6 mmol) in DMF (160 mL) and THF (80 mL) was added *t*-BuOK (1.33 g, 11.9 mmol) at −78 °C, and the mixture was stirred at −78 °C for 2 h. The reaction was quenched by the addition of 1 M NH_4Cl (50 mL). The aqueous layer was extracted with EtOAc, and the combined organic layers were washed with water and dried over $MgSO_4$. After removal of the solvent under reduced pressure, the residue was purified by column chromatography on silica gel (20:1 hexane/EtOAc) to give **A** as a pale yellow solid: ^{1}H NMR (400 MHz, $CDCl_3$) δ [ppm]: 4.54 (s, 4H), 1.44 (m, 6H), 1.14 (d, 36H, $J = 7.5$ Hz); MS (EI) *m/z* 550 [M^+].

A (2.74 g, 4.96 mmol) was placed in a 100 mL round-bottomed flask and dissolved in THF (50 mL). To the mixture was added tetrabutylammonium fluoride (1 M, 12.5 mL, 12.5 mmol) at 0 °C. After stirring for 1 h at 0 °C, the reaction was quenched by adding H_2O. The aqueous layer was extracted with EtOAc, and the combined organic layers were washed with water and dried over $MgSO_4$. After removal of the solvent under reduced pressure, the residue was purified by column chromatography on silica gel (2:1 hexane/ EtOAc) to give **3** (677 mg, 48%) as a pale yellow solid: m.p. 186–187 °C; ^{1}H NMR (400 MHz, $CDCl_3$) δ [ppm]: 8.65 (s, 2H), 4.52 (s, 4H); ^{13}C NMR (150 MHz, $CDCl_3$) δ [ppm]: 164.0, 153.2, 130.3, 103.6, 66.0; MS (EI) *m/z* 238 [M^+]. Anal. calcd. for $C_9H_6N_2S_2O_2$: C 45.36, H 2.54, N 11.76; found: C 45.19, H 2.27, N 11.57.

Synthesis of **4**: **3** (124 mg, 0.520 mmol) was placed in a 50 mL round-bottomed flask and dissolved in THF (10 mL). To the mixture was added dropwise *n*-BuLi (1.58 M, 0.7 mL) at −78 °C. After stirring for 1 h at −78 °C, $SnBu_3Cl$ (352 mg, 1.08 mmol) was added. After stirring for 0.5 h at room temperature, the reaction was quenched by the addition of H_2O (2 mL). The aqueous layer was extracted with EtOAc, and the combined organic layers were washed with water and dried over $MgSO_4$. After removal of the solvent under reduced pressure, the residue was purified by column chromatography on alumina (hexane) followed by further purification with GPC ($CHCl_3$) to give **4** (417 mg, 98%) as a yellow oil: ^{1}H NMR (400 MHz, $CDCl_3$) δ [ppm]: 4.55 (s, 4H), 1.58 (m, 12H), 1.25 (m, 24H), 0.90 (t, 18H, $J = 7.5$ Hz); ^{13}C NMR (150 MHz, $CDCl_3$) δ [ppm]: 175.6, 166.0, 133.8, 103.4, 65.5, 28.8, 27.2, 13.7, 11.5; MS (EI) *m/z* 816 [M^+].

Synthesis of C-BTz: **4** (240 mg, 0.29 mmol), 4′-bromo-2,2,2-trifluoroacetophenone (223 mg, 0.88 mmol), and tetrakis(triphenylphosphine)palladium(0) (34 mg, 0.029 mmol) were placed in a test tube and dissolved with toluene (6 mL). The reaction mixture was stirred at 120 °C for 13 h. After removal of the solvent under reduced pressure, the residue was washed with methanol and diethyl ether to give **B** (150 mg, 88%) as a red solid: ^{1}H NMR (400 MHz, $CDCl_3$) δ [ppm]: 8.15 (m, 8H), 4.62 (s, 4H); MS (EI) *m/z* 582 [M^+].

B (140 mg, 0.240 mmol) was placed in a 100 mL round-bottomed flask and dissolved with AcOH (50 mL). To the mixture was added HCl aq. (12 M, 3 mL) at 100 °C. The reaction mixture was stirred at 100 °C for 2 h. After being cooled to room temperature, the reaction was quenched by the addition of H_2O. The solid was collected and washed with H_2O, methanol, and diethyl ether followed by purification under gradient sublimation under a high vacuum (10^{-2} Pa) to give pure **C-BTz** (102 mg, 79%) as a dark green solid: m.p. > 300 °C; ^{1}H NMR (400 MHz, $CDCl_3$) δ [ppm]: 8.09 (d, 4H, $J = 8.7$ Hz), 8.07 (d, 4H, $J = 8.7$ Hz); MS (EI) *m/z* 538 [M^+]; UV–vis (THF): $\lambda_{max}^{abs}(\varepsilon) = 404$ nm (50 000); fluorescence spectra (THF): $\lambda_{max}^{ems} = 523$ nm (Φ_f 0.02). Anal. calcd. for $C_{23}H_8F_6N_2 \cdot O_3S_2$: C 51.30, H 1.50, N 5.20; found: C 51.04, H 1.41, N 5.09.

Synthesis of **5**: **1** (1.18 g, 2.46 mmol) was placed in a 200 mL round-bottomed flask and dissolved in THF (50 mL). To the mixture was added tetrabutylammonium fluoride (1 M, 9.0 mL, 9.0 mmol) at 0 °C. After stirring for 19 h at 0 °C, the reaction was quenched by the addition of H_2O. The aqueous layer was extracted with EtOAc, and the combined organic layers were washed with water and dried over $MgSO_4$. After removal of the solvent under reduced pressure, the residue was purified by column chromatography on silica gel (3:1 hexane/EtOAc) to give **5** (384 mg, 93%) as a white solid: m.p. 91–92 °C; ^{1}H NMR (400 MHz, $CDCl_3$) δ [ppm]: 8.79 (s, 2H), 8.01 (s, 2H); MS (EI) *m/z* 168 [M^+].

Synthesis of **6**: **5** (221 mg, 1.31 mmol) was placed in a 50 mL round-bottomed flask and dissolved in THF (13 mL). To the mixture was added dropwise *n*-BuLi (1.58 M, 2.5 mL, 3.95 mmol) at −78 °C. After stirring for 1 h at −78 °C, $SnBu_3Cl$ (1.02 g, 3.13 mmol) was added. After stirring for 0.5 h at room temperature, the reaction was quenched by the addition of H_2O (2 mL). The aqueous layer was extracted with EtOAc, and the combined organic layers were washed with water and dried over $MgSO_4$. After removal of the solvent under reduced pressure, the residue was purified by column chromatography on alumina (hexane) followed by further purification with GPC ($CHCl_3$) to give **6** (221 mg, 24%) as a brown oil: ^{1}H NMR (400 MHz, $CDCl_3$) δ [ppm]: 8.14 (s, 2H), 1.60 (m, 12H), 1.35 (m, 12H), 1.23 (m, 12H), 0.90 (t, 18H, $J = 7.5$ Hz); MS (EI) *m/z* 746 [M^+].

Synthesis of BTz: **6** (221 mg, 0.30 mmol), 4′-bromo-2,2,2-trifluoroacetophenone (223 mg, 0.88 mmol), and tetrakis(triphenylphosphine)palladium(0) (34 mg, 0.029 mmol) were placed in a test tube and dissolved with toluene (3 mL). The reaction mixture was stirred at 120 °C for 16 h. After being cooled to room temperature, the solvent was removed under reduced pressure. The crude solid was collected and washed with methanol and diethyl ether followed by purification under gradient sublimation at a high vacuum (10^{-2} Pa) to give pure **BTz** (35 mg, 23%) as a yellow solid: m.p. > 300 °C; ^{1}H NMR (400 MHz, $CDCl_3$) δ [ppm]: 8.19 (d, 4H, $J = 8.5$ Hz), 8.15 (d, 4H, $J = 8.5$ Hz), 8.10 (s, 2H); MS (EI) *m/z* 512 [M^+]; $\lambda_{max}^{abs}(\varepsilon) = 401$ nm (55 000); fluorescence spectra (THF): $\lambda_{max}^{ems} = 491$ nm ($\Phi_f = 0.39$). Anal. calcd. for $C_{22}H_{10}F_6N_2 \cdot O_2S_2$: C 51.56, H 1.97, N 5.47; found: C 51.32, H 1.98, N 5.70.

X-ray Information: The diffraction data of **C-BTz** were collected on a Rigaku RAXIS-RAPID Imaging Plate with monochromated Cu Kα ($\lambda = 1.54187$ Å) radiation. The structures were determined by a direct method (SHELX97). The nonhydrogen atoms were refined anisotropically.

Crystallographic Data for ***C-BTz***: $C_{23}H_8F_6N_2O_3S_2$, $M = 538.43$, triclinic, space group $P\bar{1}$ (No. 2); $a = 6.4444(3)$, $b = 9.6862(4)$, $c = 17.7387(8)$ Å; $\alpha = 98.685(2)^\circ$, $\beta = 93.765(2)^\circ$, $\gamma = 105.438(2)^\circ$; $V = 1048.56(8)$ Å^3; $Z = 2$, $D_{calcd} = 1.705$ g cm^{-3}, $F(000) = 540$, 11 150 reflections measured, 3711 unique, $R = 0.1027$ for $I > 2\sigma(I)$, $wR = 0.1154$ for all data.

Crystallographic data (excluding structure factors) for the structure reported in this paper have been deposited with the Cambridge Crystallographic Data Centre as supplementary publication no. CCDC-746339.

Bottom-Contact Device: The field-effect mobility of **C-BTz** and **BTz** was measured using a bottom-contact, thin-film, field-effect transistor (FET) geometry. The p-doped silicon substrate functioned as the gate electrode. A thermally grown silicon oxide dielectric layer on the gate substrate was 300 nm thick and a capacitance of 10.0 nF cm^{-2} was used. Interdigital source and drain electrodes were constructed with a gold (30 nm) layer formed on the SiO_2 layer. The channel width (W) and channel length (L) were 38 mm and 5 μm, respectively. The silicon oxide surface was first washed with acetone and 2-propanol. The silicon oxide surface was then activated by ozone treatment and pretreated with octadecyltrichlorosilane (ODTS). The semiconductor layer was vacuum-deposited on the Si/SiO_2 substrate at a rate of 0.2 Å s^{-1} under a pressure of 10^{-6} Pa to a thickness of 10 nm determined by a quartz crystal monitor. The characteristics of the OFET devices were measured at room temperature under a pressure of 10^{-6} Pa carefully avoiding exposure to air after fabricating of the active layer. The field-effect mobility (μ) was calculated in the saturated region at a V_{DS} of 80 V by the following equation:

$$I_{DS} = \frac{W}{2L} C_i \mu (V_{GS} - V_{th})^2 \quad (1)$$

The current on/off ratio was determined from the I_{DS} at $V_{GS} = 0$ V (I_{off}) and $V_{GS} = 100$ V (I_{on})

Top-Contact Device: The field-effect mobility of **C-BTz** and **BTz** was also measured using a top-contact thin-film field-effect transistor (FET) geometry. The n-doped silicon substrate functioned as the gate electrode. A thermally grown silicon oxide dielectric layer on the gate substrate was 300 nm thick and a capacitance of 10.0 nF cm^{-2} was used. The silicon oxide surface was first washed with acetone and 2-propanol, and then activated by ozone treatment, and pretreated with ODTS. The substrate was washed again with toluene, acetone, and 2-propanol. The semiconductor layer was vacuum-deposited on the Si/SiO_2 at a rate of 0.2 Å s^{-1} under a pressure of 10^{-6} Pa to a thickness of 10 nm determined by a quartz crystal monitor. On the top of the semiconductor layer, the gold source and drain electrodes (20 nm) were deposited by using shadow masks with a channel width of 5 mm and a channel length of 20 μm. The characteristics of the OFET devices were measured at room temperature under a pressure of 10^{-2} Pa or under atmospheric pressure in air. The field-effect mobility was calculated in the saturated region at a V_{DS} of 80 V. The current on/off ratio was determined from the I_{DS} at $V_{GS} = 0$ V (I_{off}) and $V_{GS} = 100$ V (I_{on}).

Acknowledgements

This work was supported by the Industrial Technology Research Grant Program 2008 from the New Energy and Industrial Technology Development Organization (NEDO) of Japan and a Grants-in-Aid for Scientific Research from the Ministry of Education, Culture, Sports, Science, and Technology, Japan, and by cooperative Research with Sumitomo Chemical Co., Ltd. YI is thankful to the Advanced Technology Institute Foundation and the Kinki Invention Center (Foundation). We acknowledge Masakazu Yamagishi for his assistance with the Hückel

calculations. Thanks are extended to the CAC and ISIR for their assistance in obtaining the elemental analyses. Supporting Information is available online from Wiley InterScience or from the author.

Received: September 24, 2009
Revised: November 21, 2009
Published online: February 25, 2010

[1] a) J. E. Anthony, *Chem. Rev.* **2006**, *106*, 5028. b) A. R. Murphy, J. M. J. Fréchet, *Chem. Rev.* **2007**, *107*, 1066. c) K. Takimiya, Y. Kunugi, T. Otsubo, *Chem. Lett.* **2007**, *36*, 578. d) J. E. Anthony, *Angew. Chem.* **2008**, *47*, 460; *Angew. Chem. Int. Ed.* **2008**, *47*, 452. e) A. Mishra, C.-Q. Ma, P. Bäuerle, *Chem. Rev.* **2009**, *109*, 1141.

[2] V. C. Sunder, J. Zaumseil, V. Podzorov, E. Menard, R. L. Willett, T. Someya, M. E. Gershenson, J. A. Rogers, *Science* **2004**, *303*, 1644.

[3] a) C. R. Newman, C. D. Frisbie, D. A. da Silva Filho, J.-L. Brédas, P. C. Ewbank, K. R. Mann, *Chem. Mater.* **2004**, *16*, 4436. b) A. Facchetti, M.-H. Yoon, T. J. Marks, *Adv. Mater.* **2005**, *17*, 1705.

[4] a) A. Facchetti, Y. Deng, A. Wang, Y. Koide, H. Sirringhaus, T. J. Marks, R. H. Friend, *Angew. Chem.* **2000**, *112*, 4721; *Angew. Chem. Int. Ed.* **2000,** *39*, 4547. b) A. Facchetti, M. Mushrush, H. E. Katz, T. J. Marks, *Adv. Mater.* **2003**, *15*, 33. c) G. R. Dholakia, M. Meyyappan, A. Facchetti, T. J. Marks, *Nano Lett.* **2006**, *6*, 2447.

[5] a) A. Facchetti, M.-H. Yoon, C. L. Stern, G. R. Hutchison, M. A. Ratner, T. J. Marks, *J. Am. Chem. Soc.* **2004**, *126*, 13480. b) A. Facchetti, M. Mushrush, M.-H. Yoon, G. R. Hutchison, M. A. Ratner, T. J. Marks, *J. Am. Chem. Soc.* **2004**, *126*, 13859.

[6] a) S. Ando, J-. i. Nishida, H. Tada, Y. Inoue, S. Tokito, Y. Yamashita, *J. Am. Chem. Soc.* **2005**, *127*, 5336. b) S. Ando, R. Murakami, J-. i. Nishida, H. Tada, Y. Inoue, S. Tokito, Y. Yamashita, *J. Am. Chem. Soc.* **2005**, *127*, 14996. c) D. Kumaki, S. Ando, S. Shimono, Y. Yamashita, T. Umeda, S. Tokito, *Appl. Phys. Lett.* **2007**, *90*, 053506. d) T. Kojima, J-. i. Nishida, S. Tokito, H. Tada, Y. Yamashita, *Chem. Commun.* **2007**, 1430. e) M. Mamada, J-. i. Nishida, D. Kumaki, S. Tokito, Y. Yamashita, *Chem. Mater.* **2007**, *19*, 5404. f) T. Kojima, J-. i. Nishida, S. Tokito, Y. Yamashita, *Chem. Lett.* **2007**, *36*, 1198. g) M. Mamada, J-. i. Nishida, S. Tokito, Y. Yamashita, *Chem. Lett.* **2008**, *37*, 766.

[7] a) S. Ando, J-. i. Nishida, E. Fujiwara, H. Tada, Y. Inoue, S. Tokito, Y. Yamashita, *Chem. Mater.* **2005**, *17*, 1261. b) T. Kono, D. Kumaki, J-. i. Nishida, T. Sakanoue, M. Kakita, H. Tada, S. Tokito, Y. Yamashita, *Chem. Mater.* **2007**, *19*, 1218. c) T. Kojima, J-. i. Nishida, S. Tokito, Y. Yamashita, *Chem. Lett.* **2009**, *38*, 428.

[8] a) Y. Ie, Y. Umemoto, T. Kaneda, Y. Aso, *Org. Lett.* **2006**, *8*, 5381. b) Y. Ie, M. Nitani, M. Ishikawa, K-. i. Nakayama, H. Tada, T. Kaneda, Y. Aso, *Org. Lett.* **2007**, *9*, 2115. c) Y. Ie, Y. Umemoto, M. Nitani, Y. Aso, *Pure Appl. Chem.* **2008**, *80*, 589. d) Y. Umemoto, Y. Ie, A. Saeki, S. Seki, S. Tagawa, Y. Aso, *Org. Lett.* **2008**, *10*, 1095.

[9] a) M.-H. Yoon, S. A. DiBenedetto, A. Facchetti, T. J. Marks, *J. Am. Chem. Soc.* **2005**, *127*, 1348. b) J. A. Letizia, A. Facchetti, C. L. Stern, M. A. Ratner, T. J. Marks, *J. Am. Chem. Soc.* **2005**, *127*, 13476. c) M.-H. Yoon, C. Kim, A. Facchetti, T. J. Marks, *J. Am. Chem. Soc.* **2006**, *128*, 12851. d) M.-H. Yoon, S. A. DiBenedetto, M. T. Russel, A. Facchetti, T. J. Marks, *Chem. Mater.* **2007**, *19*, 4864.

[10] X. Cai, C. P. Gerlach, C. D. Frisbie, *J. Phys. Chem. C* **2007**, *111*, 452.

[11] Y. Miyata, T. Minari, T. Nemoto, S. Isoda, K. Komatsu, *Org. Biomol. Chem.* **2007**, *5*, 2592.

[12] a) Y. Ie, Y. Umemoto, M. Okabe, T. Kusunoki, K-. i. Nakayama, Y.-J. Pu, J. Kido, H. Tada, Y. Aso, *Org. Lett.* **2008**, *10*, 833. b) Y. Ie, M. Okabe, Y. Umemoto, H. Tada, Y. Aso, *Chem. Lett.* **2009**, *38*, 460.

[13] a) T. Nakagawa, D. Kumaki, J-. i. Nishida, S. Tokito, Y. Yamashita, *Chem. Mater.* **2008**, *20*, 2615. b) M. Mamada, J.-I. Nishida, S. Tokito, Y. Yamashita, *Chem. Commun.* **2009**, 2177.

[14] T. Lee, C. A. Landis, B. M. Dhar, B. J. Jung, J. Sun, A. Sarjeant, H.-J. Lee, H. E. Katz, *J. Am. Chem. Soc.* **2009**, *131*, 1692.

[15] a) Z. Bao, A. J. Lovinger, J. Brown, *J. Am. Chem. Soc.* **1998**, *120*, 207. b) M.-M. Ling, Z. Bao, P. Erk, *Appl. Phys. Lett.* **2006**, *89*, 163 516-1.

[16] a) H. E. Katz, A. J. Lovinger, J. Johnson, C. Kloc, T. Siegrist, W. Li, Y.-Y. Lin, A. Dodabalapur, *Nature* **2000**, *404*, 478. b) H. E. Katz, J. Johnson, A. J. Lovinger, W. Li, *J. Am. Chem. Soc.* **2000**, *122*, 7787.

[17] a) B. A. Jones, M. J. Ahrens, M.-H. Yoon, A. Facchetti, T. J. Marks, M. R. Wasielewski, *Angew. Chem.* **2004**, *116*, 6523; *Angew. Chem. Int. Ed.* **2004,** *43*, 6363. b) Z. Wang, C. Kim, A. Facchetti, T. J. Marks, *J. Am. Chem. Soc.* **2007**, *129*, 13362. c) B. A. Jones, A. Facchetti, M. R. Wasielewski, T. J. Marks, *J. Am. Chem. Soc.* **2007**, *129*, 15259.

[18] a) M.-M. Ling, P. Erk, M. Gomez, M. Koenemann, J. Locklin, Z. Bao, *Adv. Mater.* **2007**, *19*, 1123. b) H. Z. Chen, M.-M. Ling, X. Mo, M. M. Shi, M. Wang, Z. Bao, *Chem. Mater.* **2007**, *19*, 816. c) M.-M. Ling, Z. Bao, P. Erk, M. Koenemann, M. Gomez, *Appl. Phys. Lett.* **2007**, *90*, 093508-1. d) R. Schmidt, M. M. Ling, J. H. Oh, M. Winkler, M. Könemann, Z. Bao, F. Würthner, *Adv. Mater.* **2007**, *19*, 3692.

[19] Y. Hosoi, D. Tsunami, H. Ishii, Y. Furukawa, *Chem. Phys. Lett.* **2007**, *436*, 139.

[20] C.-C. Kao, P. Lin, C.-C. Lee, Y.-K. Wang, J.-C. Ho, Y.-Y. Shen, *Appl. Phys. Lett.* **2007**, *90*, 212101.

[21] R. T. Weitz, K. Amsharov, U. Zschieschang, E. B. Villas, D. K. Goswami, M. Burghard, H. Dosch, M. Jansen, K. Kern, H. Klauk, *J. Am. Chem. Soc.* **2008**, *130*, 4637.

[22] a) H. Yan, Z. Chen, Y. Zheng, C. Newman, J. R. Quinn, F. Dötz, M. Kastler, A. Facchetti, *Nature* **2009**, *457*, 679. b) Z. Chen, Y. Zheng, H. Yan, A. Facchetti, *J. Am. Chem. Soc.* **2009**, *131*, 8.

[23] a) S. Handa, E. Miyazaki, K. Takimiya, Y. Kunugi, *J. Am. Chem. Soc.* **2007**, *129*, 11684. b) T. Kashiki, E. Miyazaki, K. Takimiya, *Chem. Lett.* **2009**, *38*, 568.

[24] a) H. Usta, A. Facchetti, T. J. Marks, *J. Am. Chem. Soc.* **2008**, *130*, 8580. b) H. Usta, C. Risko, Z. Wang, H. Huang, M. K. Deliomeroglu, A. Zhukhovitskiy, A. Facchetti, T. J. Marks, *J. Am. Chem. Soc.* **2009**, *131*, 5586.

[25] M. Chikamatsu, A. Itakura, Y. Yoshida, R. Azumi, Y. Yase, *Chem. Mater.* **2008**, *24*, 7365.

[26] Y. Ie, M. Nitani, Y. Aso, *Chem. Lett.* **2007**, *36*, 1326.

[27] Y. Ie, M. Nitani, T. Uemura, Y. Tominari, J. Takeya, Y. Honsho, A. Saeki, S. Seki, Y. Aso, *J. Phys. Chem. C* **2009**, *113*, 17189.

[28] M. Barbasiewicz, M. Mąkosza, *Org. Lett.* **2006**, *8*, 3745.

[29] A. J. Bard, L. R. Faulkner, in, *Electrochemical Methods–Fundamentals and Applications*, Wiley, New York, NJ **1984**.

[30] T. Mori, A. Kobayashi, Y. Sasaki, H. Kobayashi, G. Saito, H. Inokuchi, *Bull. Chem. Soc. Jpn.* **1984**, *57*, 627.

[31] Other transfer characteristics are summarized in the Supporting Information (Fig. S1, S2).

[32] The absence of a crystal structure for the **BTz** molecule made it difficult to assign these peaks.

[33] D. M. de Leeuw, M. M. J. Simenon, A. R. Brown, R. E. F. Einerhand, *Synth. Met.* **1997**, *87*, 53.

[34] T. D. Anthopoulos, G. C. Anyfantis, G. C. Papavassiliou, D. M. de Leeuw, *Appl. Phys. Lett.* **2007**, *90*, 122105.

[35] T. Yokoyama, C. B. Park, T. Nishimura, K. Kita, A. Toriumi, *Jpn. J. Appl. Phys.* **2008**, *47*, 3643.

[36] E. L. Stangeland, T. Sammakia, *J. Org. Chem.* **2004**, *69*, 2381.